Biomedical Signal Processing and Control 12 (2014) 3–9

Contents lists available at ScienceDirect

Biomedical Signal Processing and Control

journal homepage: www.elsevier.com/locate/bspc

Model interpretation of body surface potential QRST integral map variability in arrhythmia patients

György Kozmann[a], Gergely Tuboly[a,*], Zsolt Tarjányi[a], Vavrinec Szathmáry[b], Jana Švehlíková[c], Milan Tyšler[c]

[a] Department of Electrical Engineering and Information Systems, Faculty of Information Technology, University of Pannonia, Egyetem u. 10, Box 158, H-8201 Veszprém, Hungary
[b] Institute of Normal and Pathological Physiology, Slovak Academy of Sciences, Sienkiewiczova 1, 813 71 Bratislava, Slovakia
[c] Institute of Measurement Science, Slovak Academy of Sciences, Dúbravská cesta 9, 841 04 Bratislava, Slovakia

ARTICLE INFO

Article history:
Received 8 February 2013
Received in revised form 16 May 2013
Accepted 20 June 2013
Available online 22 August 2013

Keywords:
Non-dipolarity index
Numerical chest model
Numerical heart model
NDI spikes

ABSTRACT

A necessary but not sufficient prerequisite of malignant arrhythmias is the existence of elevated static or dynamic repolarization dispersion (RD) of the ventricular myocardium. The early detection of this type of spatiotemporal impairment might have a clinical importance. Body surface potential mapping, using high resolution QRST integral maps, provides a unique noninvasive method for the beat-to-beat exploration of spatial RD. The sound theoretically proven relationship of ventricular RD and QRST integral maps has been known for many years, offering a novel electrocardiological imaging possibility. However, a "yes or no" type risk assessment can be achieved even without solving the ill-posed electrocardiological inverse problem by computing the body surface potential QRST integral map non-dipolarity index (NDI). In this study a multi-element numerical heart and a piecewise homogeneous chest model was used to estimate the sensitivity of the NDIs on pathological ventricular RD patterns. The tests included the physiological RD pattern as a reference and additional 83 pathological ones classified into 3 major types. All the local action potential (AP) modulation types were systematically swept through the anterior, lateral, posterior, septal and apical segments of the left ventricle. Additionally the impact of impaired conduction system and the involvement of the right ventricle were tested as well. It was concluded that the source level origin of the extreme NDIs was located in the apical part of the heart, due to permanent myocardial necrosis, temporally refracter regions or reversed transmural AP patterns.

1. Introduction

Clinical evidences support that ventricular tachycardia (VT) and ventricular fibrillation (VF) are the most common causes of sudden cardiac death (SCD). In spite of the continuous developments (based on low ejection fraction, short and long term ECG records or exercise tests), still no reliable marker of arrhythmia prone situation does exist according to a recent scientific statement of the AHA/ACCF/HRS based on hundreds of clinical trials [1].

Alternative risk assessment methods rely on the exploitation all the information accessible on the thoracic surface noninvasively. Abildskov et al. [2] suggested body surface potential mapping for the detailed characterization of alterations of ventricular repolarization, by the use of the QRST integral maps. Hubley-Kozey et al. [3] confirmed statistically the clinical utility of QRST integral mapping in risk assessment by averaged maps. The theoretical basis of the QRST integral map-based RD detection was proven mathematically by Geselowitz [4]. Later the impulse propagation and arrhythmias was discussed in details by Kléber and Rudy [5]. Other authors emphasized the importance of beat-to-beat estimation of repolarization lability [6,7]. As a feature extraction the Karhunen–Loeve (KL) expansion based single scalar non-dipolarity index (NDI) was introduced to separate high-risk and low-risk population based on averaged QRST integral maps [8]. The dynamics of body posture associated changes in ventricular recovery was studied by Kellerová using QRST integral maps [9].

Within the new approaches it is worth mentioning the development of a simple but efficient arrhythmia vulnerability index, based on the averaged sum absolute QRST integrals of the Frank leads suggested by Tereshchenko et al. [10,11] with promising clinical performance. A different risk assessment approach based on the ECG signals of high-resolution body surface potential maps has been published recently [12,13].

In our long term pursuit for an improved non-invasive SCD risk assessment, we used body surface potential QRST integral

* Corresponding author. Tel.: +36 88 62 4224; fax: +36 88 62 4526.
E-mail addresses: kozmann.gyorgy@virt.uni-pannon.hu (G. Kozmann), tuboly.gergely@virt.uni-pannon.hu (G. Tuboly), tarjanyi@irt.vein.hu (Z. Tarjányi), Vavrinec.Szathmary@savba.sk (V. Szathmáry), umersveh@savba.sk (J. Švehlíková), umertysl@savba.sk (M. Tyšler).

1746-8094/$ – see front matter © 2013 Elsevier Ltd. All rights reserved.
http://dx.doi.org/10.1016/j.bspc.2013.06.016

maps instead of conventional ECG signals, in order to grasp all the spatial RD information accessible noninvasively on the thoracic surface [14]. The novelty in our approach was the use of beat-to-beat QRST integral map analysis instead of time-averaged QRST integral maps to characterize the stochastically changing spatial RD irregularities (lability) through the train of subsequent cardiac cycles. We could demonstrate that the non-dipolarity indices (NDI), computed from the coefficients of KL expansion of the QRST integral maps, characterize sensitively the non-dipolar beat-to-beat variability of the subsequent maps. In [14] NDI plots sensitively separated the group of implanted cardioverter (ICD) patients with documented malignant arrhythmia vulnerability from the learning group of healthy subjects. In the arrhythmia group the beat-to-beat NDI values were highly uncorrelated, the corresponding NDI amplitude histograms showed skewed lognormal distributions, sometimes with extreme NDI values going up to 0.9. In healthy subjects the sequence of NDI values were correlated and the amplitudes remained typically in the range of 0.1–0.2 with slight quasi-periodic components due to the respiration related positional heart changes.

Based on the Green's-theorem no unique conclusions can be drawn on the intramural source distributions using only the measurable body surface signals [15]. However, the relationship of body surface measurements and RD can be studied by computer models incorporating a priori knowledge provided by biological, cellular level measurements. In this conceptual study (and in its short version [16]) we attempted to give an action potential level (intramural) explanation of the observed normal and pathological NDI behaviour, with special regard to the generation of extremely large NDI spikes. To this end, numerical chest and heart models were used. We defined a model well characterizing the normal beats, subsequently step-by-step localized or extended RDs (transmural gradients) were generated by the modulation of model action potential (MoAP) parameters throughout the ventricles and their impact on the NDI sequences were analysed.

2. Materials and methods

2.1. Numerical modelling of the heart

2.1.1. Free parameters of heart geometry and action potentials

Details of the simplified computer model of the human cardiac ventricles were described previously by Szathmáry and Osvald [17]. The model was defined in a 3-dimensional matrix consisting of 1 mm^3 cubic elements. The local functional properties of the elementary volumes were represented by simplified MoAPs. The overall geometry of cardiac ventricles was defined analytically by segments of ellipsoids representing their inner (endocardial) and outer (epicardial) surfaces. The parameters of the ellipsoids were derived from the gross dimensions of the right and left ventricles (RV and LV), given as input data of the model. To simulate the fine structure of physiological repolarization heterogeneity, ventricular walls were sliced into 5 layers, paralleling with the inner and outer surfaces (Fig. 1). The different fibre directions from the endo- to epicardial myocardium were not taken into account. The MoAP characteristics of model elements may be defined differently depending on their localization in respective layers.

In the reference model, simulating the normal activation, the gross dimensions of ventricles and the parameters of activation were derived from data published by Durrer et al. [18] and Hutchins et al. [19]. Ventricular depolarization was started from predetermined elements on the inner endocardial surface of both ventricles, corresponding to regions of earliest activation (Fig. 2(a)). The spread of activation in the most inner layer, representing the Purkinje mesh, was three times faster than in the remaining layers of the walls (Fig. 2(b)). After depolarizing of model elements their consecutive repolarization is governed by their length and shape. The MoAP differences in respective layers cause a physiological transmural dispersion of cardiac action potential durations [20]. The activation and repolarization of the reference model, defined in this way corresponds well to generally accepted normal patterns of human heart activation.

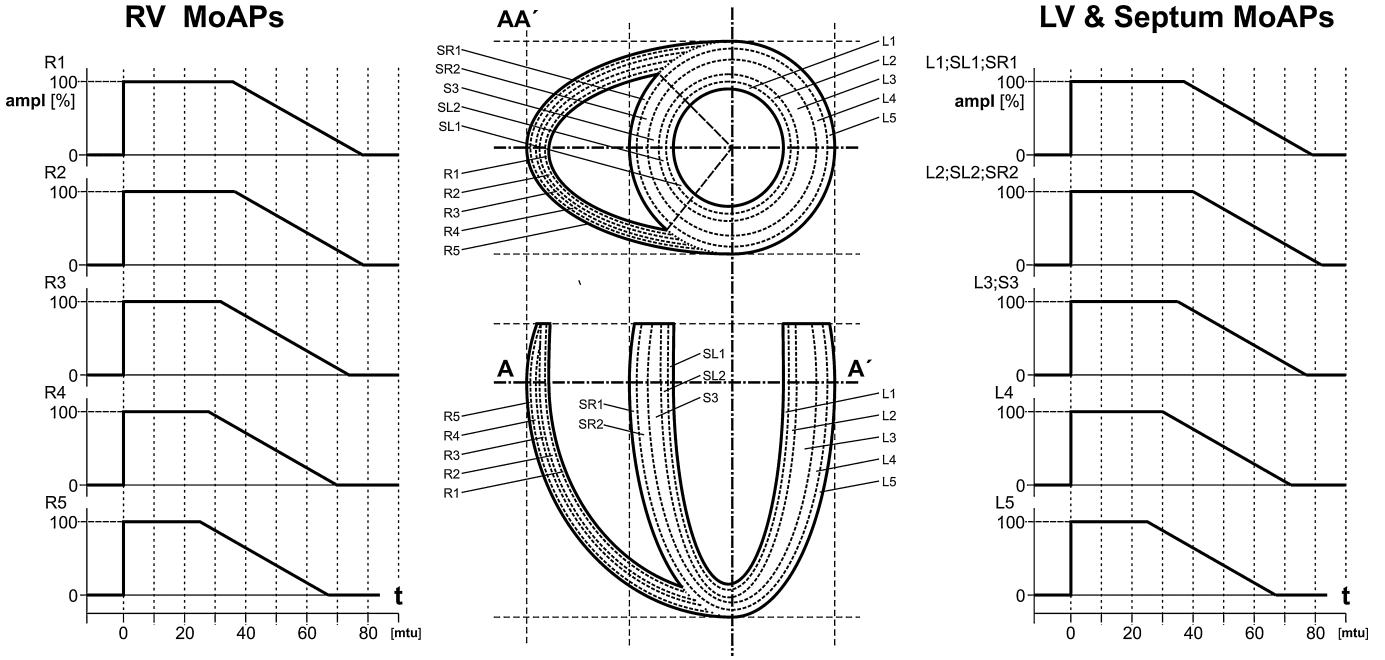

Fig. 1. A schematic representation of the "layered" structure and geometry of the left and right ventricles, with the simplified trapezoid reference model action potentials (MoAPs). Multiple layer labels next to an AP pattern (e.g. "L1; SL1; SR1") indicate same pattern for each layer. The parameters of the simplified action potentials (amplitude, plateau duration and slope gradient) are programmable.

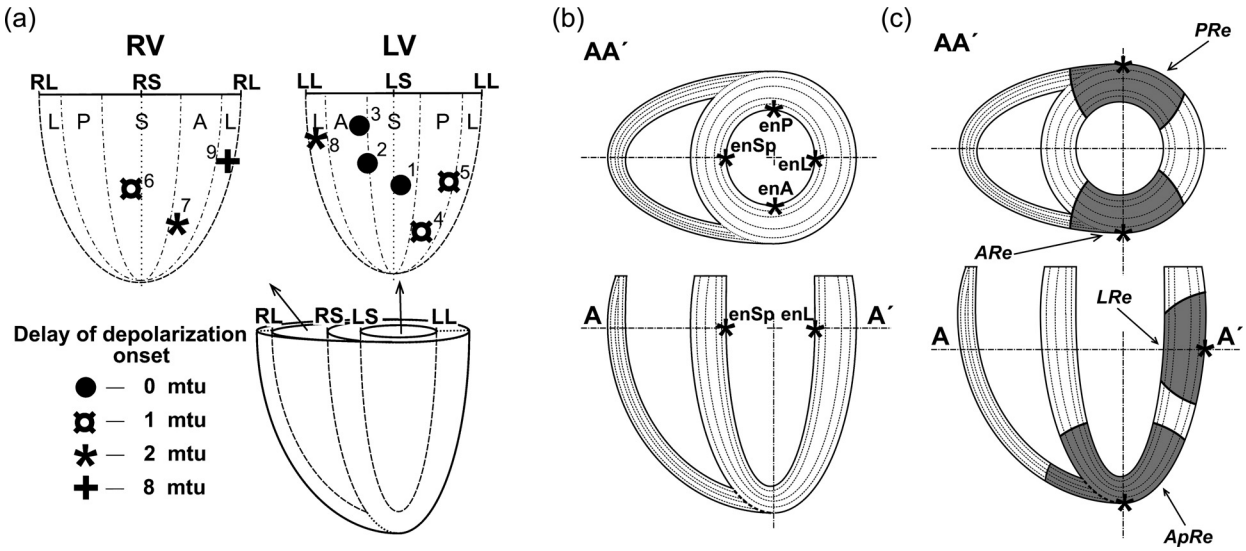

Fig. 2. Reference (a) and additional (b) activation initiation points. (a) Pacing points of the normal ventricular activation represented on the unfolded left and right endocardial surface. Symbol shapes show the sequence of normal activation onset in model time units (mtu). In this study 1 mtu was about 3 ms. Notations: lateral (L), posterior (P), septal (Sp), anterior (A) of the right and left ventricular (RV and LV) endocardial surface parts. (Notations are applied in combinations as well.) (b) Left endocardial extra pacing points with anterior (enA), lateral (enL), posterior (enP) and septal (enSp) localization. (c) Epicardial pacing points in the anterior, posterior and apical parts of the left ventricle. Shaded areas show regions with "reversed AP duration gradient" (as PRe, ARe, LRe and ApRe) due to the epicardial stimulation.

2.1.2. Options in activation and repolarization modelling

Different spatio-temporal activation and repolarization patterns were simulated by the numerical heart model. The spatio-temporal MoAP modulation focused essentially on the left ventricular myocardium, but the possible impact of bundle-branch disturbances were taken into account as well. This latter modulation was realized through the timing of activation wave initiation and by turning off certain initiation points (Fig. 2(a)). The model could also support pathological impulse pacings originated either from the endocardium or from the epicardium. The shape of ventricular tissue was unaffected by any kind of AP modulation.

2.1.3. Activation and repolarization modulation types of this study

The model allows a layer-by-layer modulation of ventricular wall repolarization parameters (Fig. 3(a)). Another option of AP modulation is shown in Fig. 3(b) where an arbitrary local segment of the myocardium has modulated AP patterns. The geometry of these local heterogeneities is defined analytically by subsidiary ellipsoids. We should remark that the wavefronts initiated from the epicardium have a "reversed gradient" of AP durations, i.e. the longest AP corresponds to the epicardial layer, the shortest to the endocardial one, if not specified otherwise (Fig. 3(a)). Application of additional pacing points is possible in arbitrary points of the myocardium if required (Fig. 2).

The spread of the activation wavefront is simulated by a cellular automaton. In each step of simulation the elementary dipole moments are computed as the potential differences between the adjacent cubic elements. Finally, the whole model of the cardiac ventricles' myocardium is divided into 33 volume segments. In each segment the dipole moments from all corresponding elements are summarized in its gravity centre, so that multiple-dipole equivalent cardiac generator is created.

2.1.4. Simulation of repolarization disparities

The aim of the simulations was to explore possible permanent or transient ventricular AP distributions behind the pathological NDI(QRST) non-dipolarity indices measured in arrhythmia patients. The set of MoAP pattern modulations is summarized below. The simulation cases are indicated in compact form. Geometry of the heart and torso were supposed the same for all simulations in each time step applying the same transfer matrix all along the cardiac cycle.

Type 1: reference (case: 1).

Type 2 modulation: Starting point, MoAP and propagation velocity parameter modulations (cases: 2–33):

- Switch-off a subset of physiological anterior and/or posterior starting points, without any changes in the MoAPs (cases: 2–5).
- Switch-off anterior (No. 2) or posterior (No. 4) starting point while the MoAP plateaus are prolonged or shortened by 40% in a small area around the relevant starting point (cases: 6–10).
- Combinations of slowing propagation velocity, with the above onset time modulations around smaller or larger areas of starting points No. 2 or No. 4 (cases: 11–22).
- Endocardial extra pacings at the mid-anterior, mid-lateral, mid-posterior and mid-septal endocardial surface simultaneously with the beginning of the regular ventricular activation onset (cases: 20–23).
- Epicardial pacings at the mid-anterior, mid-lateral and mid-posterior and mid-septal endocardial surface, with and without of AP modulations (cases: 24–33).

Type 3 modulation: Large left ventricular lesions, combined MoAP modulations (cases: 34–58):

- Modelling of large anterior, posterior and lateral lesions (cases: 34–46).
- Combined multi-parameter modulations in the left ventricle, including diffuse lesions (cases: 47–57).
- Combined multi-parameter modulations in the right ventricle (case: 58).

Type 4 modulation: Apical modulations (cases: 59–84):

- Modulations of MoAP amplitude, plateau and propagation velocity (cases: 59–64).

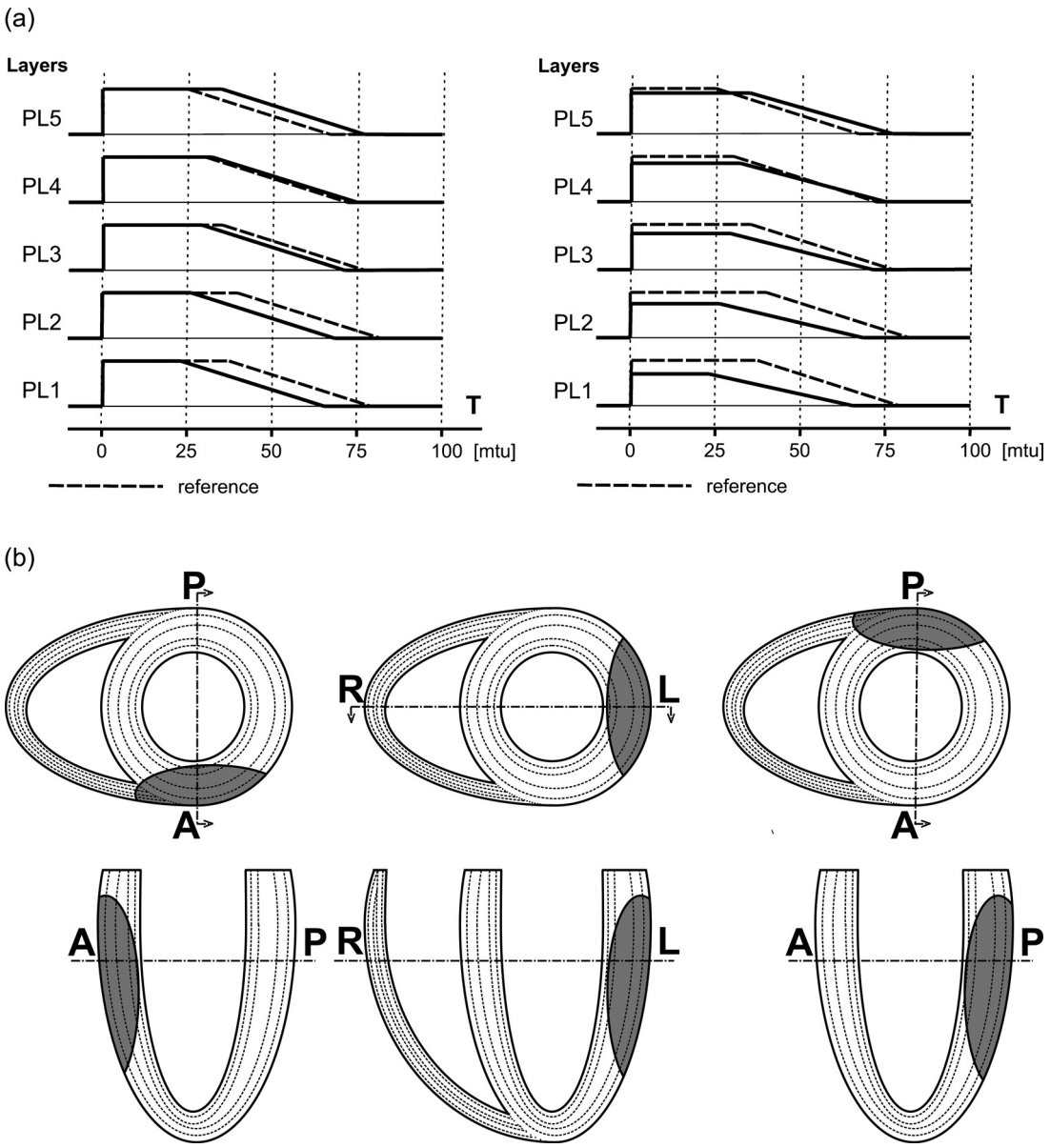

Fig. 3. (a) Examples of possible "global", "layer level" modulation of plateau length, slope gradient, amplitude of MoAPs, i.e. the specified changes/properties are valid for the whole extent of the relevant layers. (b) Modelling of lesions on the anterior (left), lateral (middle) and posterior (right) left ventricular walls. Shaded areas denote lesions.

- Simulations of subendocardial, subepicardial and transmural infarctions (cases: 65–79).
- Apical-epicardial pacing with and without of MoAP and timing modulations (cases: 80–84).

2.2. Modelling of the thorax, computation of body surface potential maps (BSPMs)

To compute the heart generated potentials on the thoracic surface, the multiple-dipole model of the cardiac generator is inserted in a realistically shaped piecewise homogeneous torso model (Fig. 4). Lungs are taken into consideration with 4× lower conductivity than general conductivity of the torso, ventricular cavities with 3× higher conductivity. The electric potentials on the body surface are computed in the surface points of the torso model using boundary element method (BEM), originally proposed by Barr et al. [21] and also used in current studies [22,23].

The use of BEM for computation of body surface potential maps $m(t)$ in Ne points on the body surface in each time instant t yields a linear matrix equation:

$$m(t) = Ag(t) \tag{1}$$

where A is the time independent transfer matrix (i.e. the geometry and position of the heart and torso were fixed during the cardiac cycle), which represents the properties of the inhomogeneous torso as volume conductor and $g(t)$ is a multiple-dipole generator (with Ns current dipoles) in a particular time step of the heart activation. The integral BSPM p representing the integral of $m(t)$ over particular time interval could then be described by (2).

$$p = \int m(t)dt = \int Ag(t)dt = A\int g(t)dt = As \tag{2}$$

where s represents the time integrals of Ns dipole moments of modelled multiple dipole generator. Considering three orthogonal components of each dipole moment, the size of the transfer matrix A is $(Ne \times 3Ns)$.

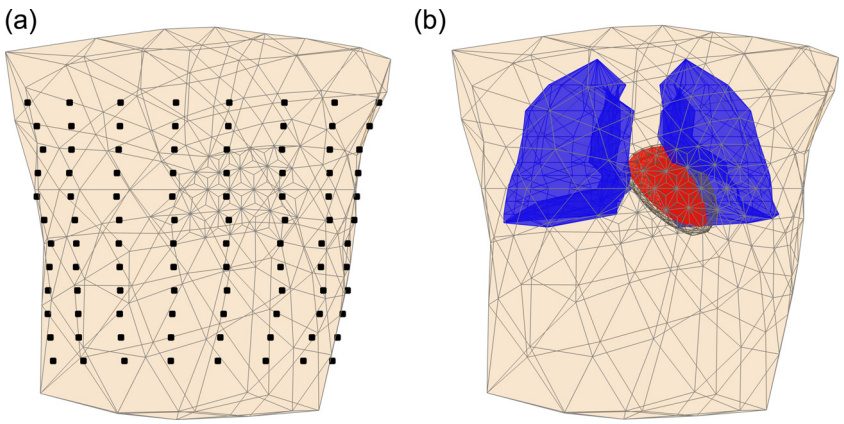

Fig. 4. (a) Realistically shaped torso model with black points indicating the frontal position of nodes in regular mesh (192 points in total), in which the BSPM is computed. (b) Piecewise homogeneous torso model configuration for simulations of BSPMs from modelled cardiac generator.

The body surface potential maps are computed from the potentials in a regular mesh (12×16) on the body surface consisting of 192 points (Fig. 4).

2.3. Evaluation of repolarization dispersion by QRST integrals and the non-dipolarity indices (NDIs)

According to Geselowitz, the amplitude of QRST integrals at an arbitrary body surface point P is a function of the AP heterogeneity, in other words, it is the function of the gradient of the μ of MoAP areas (3) of the myocardium [4]. Consequently, beat-to-beat application of (3) provides a non-invasive tool that can be used to study the spatio-temporal variability of AP properties i.e. the RD.

$$\int_{\mathrm{QRST}} \phi(P,t)dt = -k \iiint_{V_s} \mathbf{z}(P,\mathbf{r})\nabla\mu(\mathbf{r})dV_s \tag{3}$$

where

$$\mu(\mathbf{r}) = \int_{\mathrm{QRST}} [\phi_m(\mathbf{r},t) - \phi_{mr}(\mathbf{r})]\,dt \tag{4}$$

where $\phi_m(\mathbf{r},t)$ is the membrane potential at time t; $\phi_{mr}(\mathbf{r})$ is the membrane resting potential at point $\mathbf{r}$; V_s is the volume of sources (myocardium); k is a constant; and z is the vector of transfer coefficients between P and $\mathbf{r}$.

In a concise way QRST integral maps are characterized by the beat-to-beat sequence of NDI, based on the c_i components of the KL expansion.

$$\mathrm{NDI} = \frac{\sum_{i=4}^{12} c_i^2}{\sum_{i=1}^{12} c_i^2} = \frac{P_{ND}}{P_D + P_{ND}} \tag{5}$$

where P_D is the BSPM signal power represented by the "dipolar" KL components (i: 1–3) and P_{ND} is the BSPM signal power represented by the "non-dipolar" KL components (i: 4–12) according to Lux et al. [8].

3. Results

NDI values obtained by the reference (normal) activation and by the 3 types of pathological AP modulations (cases: 2–84) concisely outlined in Section 2.1.4 are shown in Fig. 5.

Type 1 modulation (case: 1). The NDI value of the reference heart beat is depicted by the first case in Fig. 5.

Type 2 modulation (cases: 2–33). The modulation of wavefront starting points and starting time instants are summarized in this type of modulations. The intermitting starting points and time instants model the impairment of the intraventricular conduction system. As starting point modulation did not change significantly the NDI values, this type of impairment remains hidden (assuming that changes in impulse propagation does not influence MoAP pattern).

- Cases between 2 and 19 reveal that disabling some ordinary initiation points or enabling extra endocardial pacing sites (ectopic beats) in the anterior, lateral, posterior and septal segments, cause only marginal NDI changes, the uncertainty due to the rotation of the heart could definitely mask this effect [9].
- On the contrary the epicardial ectopic beats (cases 20–33) generate wavefronts spreading towards the endocardium causing a reversal of the ventricular gradient, resulting in small but detectable NDI changes. According to the graph, the NDI modulation achieved is a function of the pacing site (the largest value was generated by the posterior stimulation), but essentially all the RD changes decreased the reference NDI value (negative deflections).

Type 3 modulation (cases: 34–57). Even the large extent AP modulations due to mid-wall or basal lesions caused minimal perturbation of the NDI value (with the exception of case 54), consequently the index is not an efficient indicator in these pathologies.

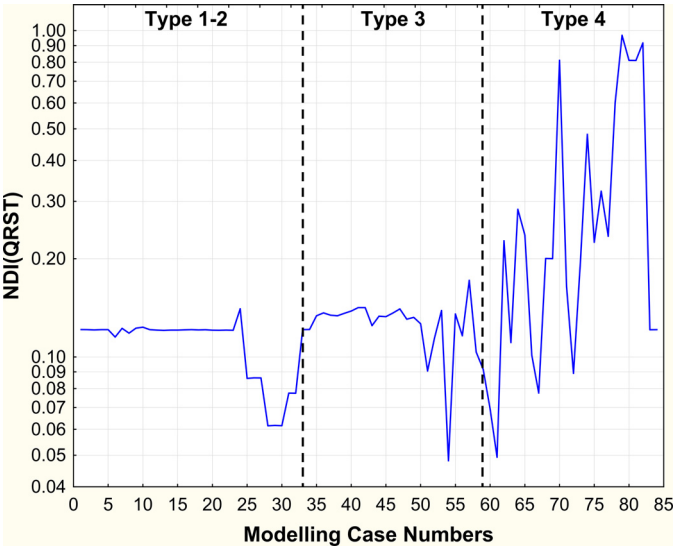

Fig. 5. Simulation cases vs. NDI values computed from QRST integral maps simulated by modelled heart-torso setup.

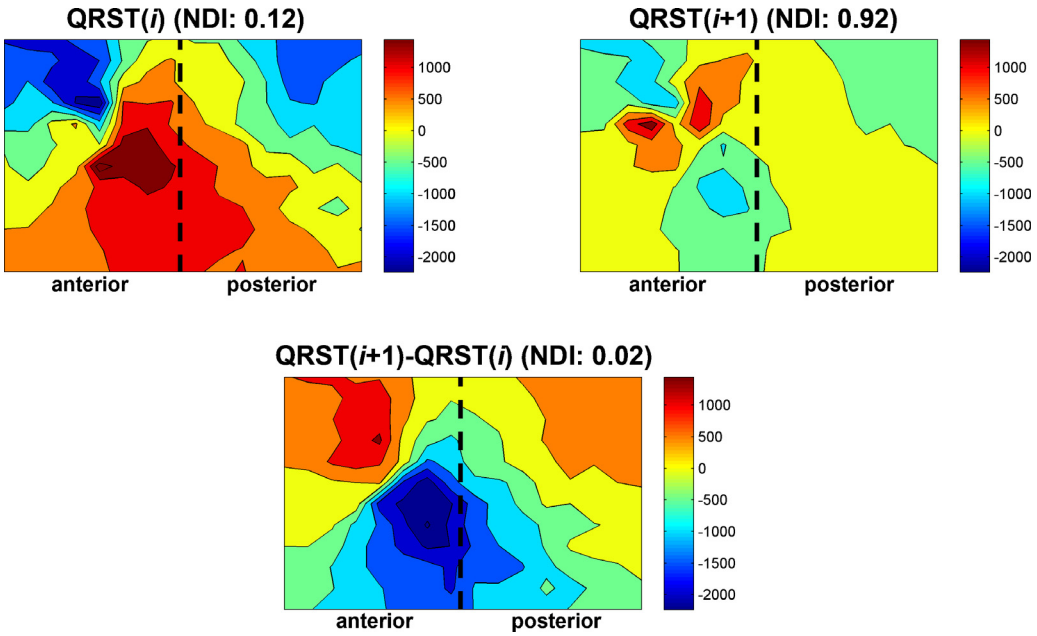

Fig. 6. Computer simulation of QRST integral maps of two subsequent cardiac cycles. The first one represents a normal (reference) beat, while the second one depicts a map modelling the QRST integral from a cycle when an epicardial ectopic wavefront launched from the apical area is superimposed on the wavefronts originating from the physiological starting points (Fig. 1(a)). In the second QRST integral map the resultant non-dipolar pattern is clearly visible. The difference of the subsequent QRST integrals (due to the superimposed ectopic beat) is essentially "dipolar" (showing the contribution of the activation front propagating inwards from the site of epicardial stimulation). Colour scale values represent relative values.

Type 4 modulation (cases: 58–86). The modelling results revealed, that the large NDI spikes frequently observable in ICD patients are generated by RD discrepancies located in the apical region. Two possible mechanisms were observed:

- According to the first one, transmural, subendocardial or subepicardial myocardial infarctions could generate large NDI deflections (cases: 60–79).
- The second mechanism of spike generations was due to apical extra activation wavefronts spreading from the epicardium to the endocardium. In the time domain these "ectopic beats" were initiated simultaneously or with a fixed delay from the initiation of the ventricular activation. The MoAP duration in this case is the largest in the firstly activated epicardial layer, gradually decreasing in the subepicardial layers, i.e. the physiological MoAP duration decreasing from the endocardium to the epicardium is reversed. However, if the MoAP durations were not following the reversed length distribution, no NDI spike was generated (see cases: 83, 84). An example of the reference integral QRST(BSPM) map followed by a map after an epicardial pacing on the apex is shown in Fig. 6.

4. Discussion

In this study the possible intramural causes of random NDI fluctuations observed in clinical measurements were simulated by the use of numerical chest and heart models. Each case in Fig. 5 represents a normal or a pathological RD heart cycle. The result of the study in statistical terms was comparable with the records of ICD patients [14]. The possible heart level source of large NDI deflections was clarified by the relationship of NDI deflection and the type of RD generated.

The aim of Type 2 modulations was to reveal the possible influence of impaired ventricular conduction system on malignant RD. This could be an important clinical issue as according to Rossi et al. [24] in aged hearts increased ventricular activation time and abnormal activation patterns are due to the impaired impulse propagation through the ventricular conduction system leading to uncoordinated endocardial excitation. The impaired interaction between the conduction system and ventricular myocardium might create a potential re-entry substrate, contributing to a higher incidence of ventricular arrhythmias in the elderly population. Unfortunately the small AP changes associated with the endocardial pacing point modulation causes only minor changes compared to the physiological one, consequently such alterations in RD remain hidden in NDI type analysis. On the contrary, changes due to epicardial stimulations are detectable. However, because the transfer coefficients between the ventricular volume elements affected by the epicardial pacing (left anterior, left lateral, left posterior) and body surface measuring points are small, NDI changes are limited.

Type 3 modulations were essentially invisible in NDI values, though permanent ischaemic changes tend to increase the NDI level. More significant changes were observed in transmural or subepicardial infarctions, including the large extent diffuse damages. Still, we may consider the observability of these pathologies by NDI alterations just borderline.

According to some Type 4 simulation experiments, high NDI values were achieved in certain transmural, subendocardial and subepicardial infarctions, or in cycles with regions still in refractory phase (cases: 64–65). However, combinations of certain AP amplitude and propagation parameters and lesions of the myocardial layers resulted in extreme NDI (case: 70). Further huge NDI deflections were generated when ectopic apical wavefronts were propagating from the epicardium to the endocardium (cases: 80–82). The latter occurred if and only if the AP durations were accompanied by a gradual decrease of AP durations from the epicardium to the endocardium. When AP durations were forced in the model to preserve the original length distributions (i.e. growing from the endocardium to the epicardium) the NDI values dropped back to the reference NDI level (see cases: 83–84).

Regarding cases 80–82, we should remark, that reversed MoAP duration provides a MoAP distribution necessary for large NDI amplitude. In real heart such an AP duration pattern is not necessarily due to a synchronized apical-epicardial pacing pulse. According

to recent studies the apical AP length gradient might be a result of the impaired coupling between the myocardial cells [25,26]. The results of the biological experiments of Zaniboni et al. [25] indicate that elevated random beat-to-beat AP duration variability is mediated by the impairment of intercellular coupling. In this case the stochastic behaviour of ion channels and the electronic interactions increase the temporal dispersion of refractoriness, i.e. we may assume that the sources generated by the epicardial ectopic beat are just equivalent with the apical AP length distribution governed by stochastic laws [27,28]. The significant random NDI spikes observable in the measurements of ICD patients make the outlined mechanisms likely.

At this point we should refer to Type 2 modulations, where similar epicardial-to-endocardial ectopic beats were applied on the mid-anterior, mid-lateral and mid-posterior regions, resulting in significant but low amplitude, negative polarity NDI spikes. In these experiments the use of epicardial QRST integral distributions could obviously reveal more irregularities of RD, but at the thoracic surface the smoothing effect of the epicardial-to-body surface transfer prevents us from obtaining the complete diagnostic information available at the heart surface. This conclusion is supported by the findings of Burnes et al. [29], verifying by experimental examples that the body surface potential distributions do not reflect the details of the patterns of epicardial integral maps.

Acknowledgements

We acknowledge the financial support of the Hungarian State and the European Union under the programmes TÁMOP-4.2.2-08/1/2008-0018, TÁMOP-4.2.2/B-10/1-2010-0025, the financial support of the Slovak Research and Development Agency under the programme APVV-0513-10 and of the financial support of VEGA Grant Agency, Slovakia under the programme 2/0131/13.

The publication is supported by the European Union and co-funded by the European Social Fund.

Project title: “Telemedicine-focused research activities in the field of Mathematics, Informatics and Medical sciences”; Project number: TÁMOP-4.2.2.A-11/1/KONV-2012-0073.

References

[1] J.J. Goldberger, M.E. Cain, S.H. Hohnloser, A.H. Kadish, B.P. Knight, M.S. Lauer, B.J. Maron, R.L. Page, R.S. Passman, D. Siscovick, W.G. Stevenson, D.P. Zipes, American Heart Association/American College of Cardiology Foundation/Heart Rhythm Society Scientific Statement on Noninvasive Risk Stratification Techniques for Identifying Patients at Risk for Sudden Cardiac Death: A scientific statement from the American Heart Association Council on Cardiology Committee on Electrocardiography and Arrhythmias and Council on Epidemiology and Prevention, Circulation 118 (2008) 1497–1518.

[2] J.A. Abildskov, L.S. Green, A.K. Evans, R.L. Lux, The QRST deflection area of electrograms during global alterations of ventricular repolarization, Journal of Electrocardiology 15 (1982) 103–107.

[3] C.L. Hubley-Kozey, L.B. Mitchell, M.J. Gardner, J.W. Warren, C.J. Penney, E.R. Smith, B.M. Horácek, Spatial features in body-surface potential maps can identify patients with a history of sustained ventricular tachycardia, Circulation 92 (1995) 1825–1838.

[4] D.B. Geselowitz, The ventricular gradient revisited: relation to the area under the action potential, IEEE Transactions on Biomedical Engineering 30 (1983) 76–77.

[5] A.G. Kléber, Y. Rudy, Basic mechanisms of cardiac impulse propagation and associated arrhythmias, Physiological Reviews 84 (2004) 431–488.

[6] R.D. Berger, E.K. Kasper, K.L. Baughman, E. Marban, H. Calkins, G.F. Tomaselli, Beat-to-beat QT interval variability: novel evidence for repolarization lability in ischemic and nonischemic dilated cardiomyopathy, Circulation 96 (1997) 1557–1565.

[7] W.L. Atiga, H. Calkins, J.H. Lawrence, G.F. Tomaselli, J.M. Smith, R.D. Berger, Beat-to-beat repolarization lability identifies patients at risk for sudden cardiac death, Journal of Cardiovascular Electrophysiology 9 (1998) 899–908.

[8] R.L. Lux, A.K. Evans, M.J. Burgess, R.F. Wyatt, J.A. Abildskov, Redundancy reduction for improved display and analysis of body surface potential maps. I. Spatial compression, Circulation 49 (1981) 186–196.

[9] E. Kellerová, V. Szathmáry, G. Kozmann, K. Haraszti, Z. Tarjányi, Spontaneous variability and reactive postural beat-to-beat changes of integral ECG body surface potential maps, Physiological Research 59 (2010) 887–896.

[10] L.G. Tereshchenko, A. Cheng, B.J. Fetics, J.E. Marine, D.D. Spragg, S. Sinha, H. Calkins, G.F. Tomaselli, R.D. Berger, Ventricular arrhythmia is predicted by sum absolute QRST integral but not by QRS width, Journal of Electrocardiology 43 (2010) 548–552.

[11] L.G. Tereshchenko, A. Cheng, B.J. Fetics, B. Butcher, J.E. Marine, D.D. Spragg, S. Sinha, D. Dalal, H. Calkins, G.F. Tomaselli, R.D. Berger, A new electrocardiogram marker to identify patients at low risk for ventricular tachyarrhythmias: sum magnitude of the absolute QRST integral, Journal of Electrocardiology 44 (2011) 208–216.

[12] B. Khaddoumi, H. Rix, O. Meste, M. Fereniec, R. Maniewski, Body surface ECG signal shape dispersion, IEEE Transactions on Biomedical Engineering 53 (2006) 2491–2500.

[13] M. Fereniec, G. Stix, M. Kania, T. Mroczka, D. Janusek, R. Maniewski, Risk assessment of ventricular arrhythmia using new parameters based on high resolution body surface potential mapping, Medical Science Monitor 17 (2011) 26–33.

[14] G. Kozmann, K. Haraszti, I. Préda, Beat-to-beat interplay of heart rate, ventricular depolarization, and repolarization, Journal of Electrocardiology 4 (3) (2010) 15–24.

[15] R.M. Gulrajani, Bioelectricity and Biomagnetism, John Wiley & Sons, New York, 1998.

[16] G. Kozmann, Z. Tarjányi, G. Tuboly, V. Szathmáry, J. Švehlíková, M. Tyšler, Model interpretation of non-dipolar integral body surface QRST maps randomly appearing in arrhythmia patients, in: 8th IFAC Symposium on Biological and Medical Systems proceedings (on CD), 2012, pp. 1–5.

[17] V. Szathmáry, R. Osvald, An interactive computer model of propagated activation with analytically defined geometry of ventricles, Computers and Biomedical Research 27 (1994) 27–38.

[18] D. Durrer, R.T.H. Van Dam, G.E. Freud, M.J. Janse, F.L. Meijler, R.C. Arzbaecher, Total excitation of the isolated human heart, Circulation 41 (1970) 899–912.

[19] G.M. Hutchins, B.H. Bulkley, G.W. Moore, M.A. Piasio, F.T. Lohr, Shape of the human cardiac ventricles, American Journal of Cardiology 41 (1978) 646–654.

[20] M.R. Franz, K. Bargheer, W. Rafflenbeul, A. Haverich, P.R. Lichtlen, Monophasic action potential mapping in human subjects with normal electrocardiograms: direct evidence for the genesis of the T wave, Circulation 75 (1987) 379–386.

[21] R.C. Barr, T.C. Pilkington, J.P. Boineau, M.S. Spach, Determining surface potentials from current dipoles, with application to electrocardiography, IEEE Transactions on Biomedical Engineering 13 (1966) 88–92.

[22] M. Tyšler, M. Turzová, M. Tiňová, J. Švehlíková, E. Hebláková, V. Szathmáry, S. Filipová, Use of body surface potential maps for model-based assessment of local pathological changes in the heart, Bulletin of the Polish Academy of Sciences: Technical Sciences 53 (2005) 207–215.

[23] M. Stenroos, The transfer matrix for epicardial potential in a piece-wise homogeneous thorax model: the boundary element formulation, Physics in Medicine and Biology 54 (2009) 5443–5455.

[24] S. Rossi, S. Baruffi, A. Bertuzzi, M. Miragoli, D. Corradi, R. Maestri, R. Alinovi, A. Mutti, E. Musso, A. Sgoifo, D. Brisinda, R. Fenici, E. Macchi, Ventricular activation is impaired in aged rat hearts, Heart and Circulatory Physiology: American Journal of Physiology 295 (2008) 336–347.

[25] M. Zaniboni, A.E. Pollard, L. Yang, K.W. Spitzer, Beat-to-beat repolarization variability in ventricular myocytes and its suppression by electrical coupling, Heart and Circulatory Physiology: American Journal of Physiology 278 (2000) 677–687.

[26] E. Pueyo, A. Corrias, L. Virág, N. Jost, T. Szél, A. Varró, N. Szentandrássy, P.P. Nánási, K. Burrage, B. Rodríguez, A multiscale investigation of repolarization variability and its role in cardiac arrhythmogenesis, Biophysical Journal 101 (2011) 2892–2902.

[27] D.M. Jonson, J. Heijman, E.F. Bode, D.J. Greensmith, H. van der Linde, N. Abi-Gerges, D.A. Eisner, A.W. Trafford, P.G. Volders, Diastolic spontaneous calcium release from the sarcoplasmic reticulum increases beat-to-beat variability of repolarization in canine ventricular myocytes after β-adrenergic stimulation, Circulation Research 112 (2013) 246–256.

[28] A.V. Glukhov, V.V. Fedorov, Q. Lou, V.K. Ravikumar, P.W. Kalish, R.B. Schuessler, N. Moazami, I.R. Efimov, Transmural dispersion of repolarization in failing and nonfailing human ventricle, Circulation Research 106 (2010) 981–991.

[29] J.E. Burnes, R.N. Ghanem, A.L. Waldo, Y. Rudy, Imaging dispersion of myocardial repolarization. I. Comparison of body-surface and epicardial measures, Circulation 104 (2001) 1299–1305.